HHS Public Access

Author manuscript

ACS Nano. Author manuscript; available in PMC 2017 November 02.

Published in final edited form as:

ACS Nano. 2017 August 22; 11(8): 7747–7757. doi:10.1021/acsnano.7b01239.

Nanoporous Immunoprotective Device for Stem-Cell-Derived β-Cell Replacement Therapy

Ryan Chang[†,iD], **Gaetano Faleo**[§], **Holger A. Russ**[‖,⊥], **Audrey V. Parent**[‖], **Susanna K. Elledge**[‡], **Daniel A. Bernards**[‡], **Jessica L. Allen**[‡], **Karina Villanueva**[‖], **Matthias Hebrok**[‖], **Qizhi Tang**[§,‖], and **Tejal A. Desai**[*,†,‡]

[†]UCSF-UC Berkeley Joint PhD Program in Bioengineering, San Francisco, California 94143, United States

[‡]Department of Bioengineering and Therapeutic Sciences, University of California, San Francisco, San Francisco, California 94143, United States

[§]Department of Surgery, University of California, San Francisco, San Francisco, California 94143, United States

[‖]Diabetes Center, University of California, San Francisco, San Francisco, California 94143, United States

Abstract

Encapsulation of human embryonic stem-cell-differentiated beta cell clusters (hES-βC) holds great promise for cell replacement therapy for the treatment of diabetics without the need for chronic systemic immune suppression. Here, we demonstrate a nanoporous immunoprotective polymer thin film cell encapsulation device that can exclude immune molecules while allowing exchange of oxygen and nutrients necessary for *in vitro* and *in vivo* stem cell viability and function. Biocompatibility studies show the device promotes neovascular formation with limited foreign

[*]**Corresponding Author**, tejal.desai@ucsf.edu.

ORCID

Ryan Chang: 0000-0003-4052-3271

[⊥]**Present Address**, Barbara Davis Center for Diabetes, University of Colorado, School of Medicine, Aurora, CO 80045, USA.

ASSOCIATED CONTENT

Supporting Information

The Supporting Information is available free of charge on the ACS Publications website at DOI: 10.1021/acsnano.7b01239.

Gross image and SEM of fabricated nanoporous cell encapsulation device, activation of splenocyte-secreted cytokine diffusion across immunoprotective barriers, insulin GFP reporter fluorescent intensity and live cell image, protein adsorption characterization, histology of subcutaneous polymer implants, generation of $hES^{INS\text{-}GFP;AAVS1\text{-}LUC}$ cell line, histological analysis of teratoma cells confined by device, assessment of optimal transplant site for device-encapsulated stem cells (PDF)

Author Contributions

R.C., G.F., Q.T., and T.D. designed experiments. R.C. and D.A.B. fabricated membranes. R.C. and S.K.E. performed *in vitro* experiments in characterizing membranes. J.L.A. performed SEM analysis. G.F. performed *in vivo* transplants. R.C. and G.F. performed *in vivo* experiments of cell encapsulation implants. H.A.R. and A.V.P. performed differentiation of stem-cell-derived beta cell clusters. R.C., G.F., and Q.T. analyzed the data, and R.C. wrote the manuscript. M.H., Q.T., and T.A.D. provided direction and supervised the project. H.A.R., A.V.P., D.A.B., M.H., Q.T., and T.A.D. edited the manuscript.

The authors declare the following competing financial interest(s): T.D. is a scientific founder of Encellin Inc., a cell therapy device company. Q.T. is a consultant for Encellin. M.H. is on the scientific advisory board of Encellin. The University of California, San Francisco (UCSF) has filed a provisional patent application on this macroencapsulation technology for cell-based therapy.

body response *in vivo*. The device also successfully prevented teratoma escape into the peritoneal cavity of mice. Long-term animal studies demonstrate evidence of engraftment, viability, and function of cells encapsulated in the device after 6 months. Finally, *in vivo* study confirms that the device was able to effectively immuno-isolate cells from the host immune system.

Graphical Abstract

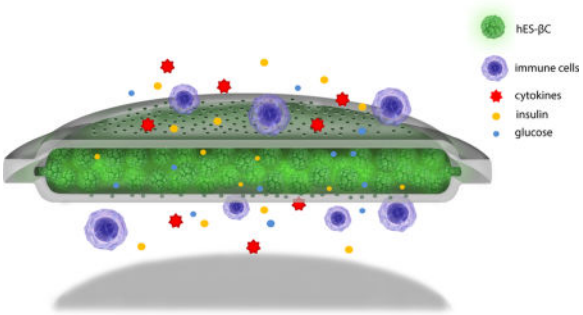

Keywords

cell encapsulation device; cell therapy; nanotechnology; immunoengineering; diabetes

Diabetes mellitus is a disease characterized by autoimmune-mediated β-cell destruction in type 1 diabetes and progressive β-cell dysfunction in type 2 diabetes, leading to insulin insufficiency. The current standard of care for diabetics relies on closely monitoring blood glucose levels and administration of exogenous insulin by injections to simulate natural insulin secretion kinetics of pancreatic β cells. However, exogenous insulin delivery often fails to adequately modulate blood glucose levels within a tight physiological range. Resulting complications include life-threatening hypoglycemic episodes and hyperglycemia-induced long-term micro- and macroangiopathies, leading to cardiovascular pathologies, kidney failure, retinopathy, and neuropathy.[1] Pancreas and pancreatic islet transplantation has been proven to be an effective treatment modality for T1D patients to achieve insulin independence;[2–4] however, its use has been limited due to islet donor shortages and the need for chronic systemic immune suppression.[5]

The development of human embryonic stem cell (hES) or induced pluripotent stem cells (iPSC)-derived insulin-producing cells promises to address the challenge of islet donor shortage.[6] Although several groups have successfully produced insulin-secreting cells from hES and iPSC,[7–14] clinical translation requires new engineering solutions to address safety concerns of teratoma formation and protection against immune rejection.[15] Cell encapsulation has emerged as a promising strategy by providing a physical barrier between transplanted hES-derived beta cell clusters (hES-βC) and the transplant recipient, thereby achieving immunoprotection from the host immune response.[16,17] The optimal cell encapsulation device should allow sufficient oxygen and nutrient exchange in order to support the viability of encapsulated cells. It should also allow for efficient transport of glucose and insulin so that blood glucose can be properly controlled. At the same time, immunoprotective cell encapsulation devices need to exclude penetration of immune cells,

antibodies, and proinflammatory cytokines. The devices must also be biocompatible and should confine any potentially tumorigenic cells.

Over the years, there have been several reports of macro- or microencapsulation strategies for islet transplantation that have achieved varying degrees of success.[18–22] A microencapsulation approach uses a polymer to individually contain a single cell or islet cluster within a microscale capsule, in order to maximize the surface area to volume ratio for improved nutrient exchange.[23] However, there is limited control over the thickness and pore size of microcapsules, and retrieval after injection is difficult. On the other hand, macroencapsulation devices that contain many cells or islet clusters allow for much greater control over membrane thickness and pore size and can be readily retrieved after transplantation. However, these devices are suboptimal in nutrient exchange owing to thicker membranes and larger reservoir volume.[24] One of the most challenging constraints is straddling the encapsulation device diffusional barrier between the limits of cell viability and adequate immune protection. It is useful to characterize the diffusional properties of cell encapsulation barriers by their ability to transport immunoglobulins, proinflammatory cytokines, insulin, and glucose as a way of instructing future encapsulation device designs. In our previous work, we demonstrated the initial proof of concept of these thin film devices to encapsulate and protect the immortalized MIN6 cell line.[25,26]

In this report, we incorporate hES-βC into an immunoprotective macroencapsulation device. We specifically show that the membranes are able to exclude proinflammatory cytokines while allowing sufficient glucose and insulin exchange. Furthermore, we also demonstrate favorable long-term *in vivo* biocompatibility of the device as characterized by low foreign body response, robust neovasculature formation, and the ability to prevent cellular escape leading to teratomas. Encapsulated hES-derived insulin-producing cells were shown to be viable and have measurable glucose-sensitive C-peptide response in mice 6 months after transplantation. Finally, the immunoprotective devices successfully prevented the priming of antigen-specific T cells *in vivo*.

RESULTS AND DISCUSSION

Immunoprotective Cell Encapsulation Device Design and Fabrication

The immunoprotective cell encapsulation device should allow for exchange of insulin, glucose, and oxygen while excluding immune cells, immunoglobulins, and proinflammatory cytokines across the membrane barrier (Figure 1A). A bilaminar nanoporous thin film macroencapsulation device is a favorable design due to its ability to minimize inward transport of immune species through tightly controlled pore structures, whereas the thin film barrier reduces the diffusional distance for optimal exchange of oxygen and nutrients. Proinflammatory cytokines interleukin-1beta (IL-1β), interferon-gamma (IFNγ), and tumor necrosis factor-alpha (TNFα) have hydrodynamic radii of 2.18, 3.67, and 3.80 nm, respectively;[27–29] therefore, immunoprotective membranes require pore diameters on the order to 10 to 100 nm. Polycaprolactone, a synthetic polymer, was selected as the preferred material owing to its favorable physical and biocompatibility properties.[30] Unlike natural polymers such as sodium alginate that have batch-to-batch variations and are often contaminated with endotoxins,[31] synthetic polymer can be synthesized under reproducible

and endotoxin-free conditions.[32] Polycaprolactone has also been used in a variety of FDA-approved medical products.[30] Furthermore, the low melting temperature of polycaprolactone allows for precise templating of stringently controlled pore sizes as well as tailored design of device geometry and thickness.

We fabricated nanoporous immunoprotective membranes (NIM) using a substrate templating technique (Figure 1B).[25] Briefly, zinc oxide nanorods were grown hydrothermally onto silicon wafers to yield structures measuring 20 nm in diameter and 500 nm in height (Figure 1C). Polycaprolactone (PCL) solution was spin-cast onto zinc oxide nanotemplated silicon substrates (Figure 1D), followed by sulfuric acid etching of zinc oxide. The resulting polymer membrane is a 10 μm thick, consisting of a 500 nm thick nanoporous layer backed by a supporting porous layer (Figure 1E). These membranes are highly flexible and mechanically stable to permit the assembly of the nanoporous immunoprotective device (NID) for cell encapsulation. Two NIMs are cut to desired shapes and heat-sealed at 70 °C along the edges to form a bilaminar flexible and nonbrittle device with mechanical integrity that can be easily handled with forceps (Figure 1F and Supplementary Figure 1A,B).

In Vitro Characterization of Nanoporous Immunoprotective Membranes

Immunoprotective barriers designed for cell encapsulation must selectively inhibit diffusion of key immunogenic molecules including immunoglobulins and proinflammatory cytokines while permitting exchange of glucose and insulin. Human IgG has a molecular weight of 153 kDa[33] whereas the TNFα homotrimer, IFNγ, and IL-1β proinflammatory cytokines have molecular weights of 52, 17, and 30 kDa, respectively.[27–29] Twenty nanometers and 200 nm pore size NIMs (NIM-20 and NIM-200, respectively) were fabricated and characterized for their robust ability to prevent diffusion of immunoglobulins and proinflammatory cytokines. In addition, we included 400 nm PTFE membranes (PTFE-400) with pore size comparable to that of the Theracyte device,[34] the first macroencapsulation device to be tested in clinical studies, as a control. We studied the molecular weight diffusion cutoff limit of NIMs and PTFE-400 by evaluating the diffusion rate of 4, 10, and 40 kDa dextran molecules over a course of 7 days at physiological 37 °C. Both NIM-20 and NIM-200, but not PTEF-400, were successful in preventing transport of 4, 10, and 40 kDa dextran molecules (Figure 2A). Whereas NIMs are able to inhibit diffusion of high molecular weight cytokines, it is critical that they do not hinder the transport of smaller molecules such as glucose. We measured the amount of glucose diffusion across NIM-20, NIM-200, and PTFE-400 over 5 min at 37 °C incubation. There was no significant difference between the amount of glucose transported across the three groups (Figure 2B). These membrane characterization studies suggest that NIMs preferentially exclude larger molecular weight species such as immunoglobulin and proinflammatory cytokines while permitting the diffusion of smaller molecules, including glucose.

To determine if NIMs can selectively block immune molecules, we first investigated the ability of NIMs to inhibit diffusion of human IgG over 1 week of 37 °C incubation. In this study, PTFE-400 failed to prevent transport of IgG while both NIM-20 and NIM-200 significantly reduced IgG transport (Figure 2C). We furthered investigated which cytokines were preferentially excluded from diffusing into the cell-containing compartment using a

mouse proinflammatory cytokine Luminex panel.[35] We observed reduced cytokine diffusion across NIM-20 relative to NIM-200 or PTFE-400 barriers following a 7 day diffusion study (Figure 2D). Interestingly, certain cytokines were excluded more effectively than others. For instance, only 10% of IL-1β was transported across NIM-20 while 25 and 80% of TNFα and IFNγ were transported across the same NIM-20, respectively. One may expect a size-dependent relationship that can explain the diffusion profile of our panel of proinflammatory cytokines. Cytokine diffusion rates were compared against their respective protein molecular weights (Figure 2E). Although there was a general trend toward reduced diffusion with larger molecular weight cytokines, there exists a population of small molecular weight cytokines with poor transport kinetics. One of the properties explaining this phenomenon could be differences in protein charges as the negatively charged polycaprolactone NIMs[30] can preferentially cause adhesion of positively charged cytokines. Indeed, the isoelectric point of cytokines had a significant effect on the protein's ability to transport across NIMs. Specifically, cytokines with isoelectric points above 7 that are positively charged at neutral pH transported poorly across NIMs regardless of their molecular weight, while negatively charged cytokines exhibited size-dependent transport kinetics (Figure 2E). Electrostatic repulsion between the cytokines and the surface of the polymer nanopores potentially allows negatively charged cytokines to traverse through the nanoporous structures of NIMs more effectively.

Because cytokine diffusion is attenuated, we then further determined if NIMs offer pancreatic islets protection against cytokine exposure. In a transwell coculture system, mouse islets were placed in the top compartment, and syngeneic mouse splenocytes activated by surface-immobilized anti-CD3 and anti-CD28 were placed in the bottom compartment as a source of cytokines. The top and bottom compartments were separated by NIM-20 and NIM-200 or a 8 μm PTFE barrier (PTFE-8000). The viability of mouse islets was quantified 48 h later using flow cytometry of dissociated islets after propidum iodine staining. Results of this study demonstrate significantly reduced apoptosis in mouse islets protected by NIM-20 and NIM-200 when compared to islets protected by PTFE-8000 (Figure 2F). Consistent with our results shown in Figure 2D, we confirmed that NIM-20 reduced proinflammatory cytokine diffusion into the islet compartment (Supplementary Figure 2A).

In Vitro Evaluation of Cell Viability and Function in Nanoporous Immunoprotective Devices

Once establishing that the exclusion of cytokines and immunoglobulins is important for preservation of primary mouse islet viability, we evaluated the ability of NIDs to support the viability and function of encapsulated human stem-cell-derived beta cell clusters as a more relevant system for cell therapy approaches. hES-βC cells were generated by a direct differentiation approach previously described[8] with modifications of the last stage based on published work.[14,36] To facilitate the detection of hES-βC, we generated them from Mel1 human embryonic stem cells that contain a GFP reporter driven under the endogenous insulin promoter.[37] Using this cell line, endogenous insulin expression, and thus β-cell viability, can be followed live by measuring the GFP fluorescence signal. Differentiated clusters consist of approximately 35% hES-βC cells as identified by intracellular flow analysis for human C-peptide as a readout of endogenous insulin production (Figure 3A). In

addition, virtually all hES-βC cells coexpress key β-cell transcription factors PDX1 and NKX6.1 (Figure 3A), shown to be critical for β-cell function and maintenance.[38,39] To further characterize our NIMs, we delivered hES-βC 300 clusters to the luminal cavity of a partially sealed NID where they are then fully encapsulated by localized heat sealing (Figure 3B). The heat is well localized during the sealing procedure, and cells remain viable and well distributed within the bilaminar NID device following encapsulation (Supplementary Figures 1A and 3B). Importantly, fluorescence intensity from NID-encapsulated hES-βC was stable in both NID-20 and NID-200 over a course of 5 weeks *in vitro* (Figure 3C and Supplementary Figure 3A). This result demonstrates that insulin expression and thus viability of hES-βC encapsulated in NID can be maintained in culture over prolonged periods of time. We further studied the ability of NID-encapsulated hES-βC to secrete insulin in response to glucose stimulations. Interestingly, both NID-20- and NID-200-encapsulated hES-βC exhibited glucose-stimulated insulin secretion with comparable glucose stimulation indices (GSI) of approximately 1.5 (Figure 3D,E). While these data are within the range of GSI reported previously,[8,14,36] it is likely that insulin diffusion was somewhat restricted as we observed reduced C-peptide concentration in both high and low glucose buffers in the smaller pore size NID-20 compared to that of NID-200. Based on these results, we continued our studies with NID-200 as it represents a more ideal encapsulation device for further animal studies because it protected islets against immunological challenges and allowed better diffusion of small molecules, including insulin and glucose.

In Vivo NID Biocompatibility and Prevention of Teratoma Escape

Biocompatibility of biomaterials has been shown to be critical for the safety and integrity of long-term cell encapsulation devices.[40] In particular, foreign body responses and fibrous capsule development following implantation of medical devices need to be carefully studied for NIDs. Protein adsorption on material surfaces can promote macrophage recruitment to the tissue−material implant site, which may become activated through the alternative pathway and enhance fibrogenesis by fibroblasts, leading to fibrous capsule formation around the implant.[41,42] To study this property, we incubated PCL and PTFE surfaces in fetal bovine serum for 24 h and demonstrate similar levels of protein adsorption on both material surfaces (Supplementary Figure 4A). An ideal biomaterial for cell encapsulation implant devices should exhibit low macrophage recruitment and fibrosis at the material −tissue interface while also permitting the formation of neovasculature along the surface of the material to provide oxygen and nutrient support for the encapsulated cells. To this end, polycaprolactone and polypropylene (PP) films were implanted subcutaneously into immunocompetent C57BL/6J mice as part of a long-term *in vivo* biocompatibility study. Implanted PCL films along with surrounding tissue were explanted at 1 month followed by tissue sectioning and H&E staining. In addition, a 4 month *in vivo* biocompatibility study was performed in the same manner, and skin tissues were sectioned and immunostained for collagen 1, a macrophage marker (F4/80), and von Willibrand Factor to elucidate fibrosis, macrophage recruitment, and angiogenesis, respectively. H&E stainings demonstrate the robust deposition of fibrotic tissue and infiltration of immune cells in tissue with polypropylene implant. On the contrary, whereas there is some infiltration of immune cells in the polycaprolactone implant, there is no deposition of fibrotic tissue along the graft

(Figure 4A). Immunostainings show increased blood vessel formation and reduced fibrosis and macrophage recruitment in PCL film grafts compared to PP implants (Figure 4B). These data are in agreement with H&E staining (Supplementary Figure 5A,B) that showed minimal fibrosis following 4 month subcutaneous transplant in immunocompetent mice and suggest that PCL thin films exhibit favorable biocompatibility, leading to robust neovasculature formation in the absence of chronic foreign body response.

The use of cell encapsulation devices for the transplantation of human stem cell products is important due to regulatory safety considerations in the event of cell escape, dedifferentiation, and/or teratoma formation. Macroencapsulation devices are advantageous over microencapsulation strategies because they prevent the distribution of stem cells throughout the body and allow for easier retrieval of explant. This is particularly important for the prevention of teratomas which can arise from hES cells that are not fully differentiated.[43] We modeled the formation of teratomas *in vivo* by transplanting either encapsulated or naked undifferentiated hES into immune-deficient NOD scid gamma (NSG) mice. Encapsulated hES cells were transplanted between the caudate lobe and left hepatic lobe, and naked cells were delivered under the kidney capsule in order to confine their location within the animal.[44] To be able to efficiently monitor hES cells after transplantation into animals, we engineered a constitutively expressed firefly luciferase gene into the insulated human AAVS1 loci of Mel1$^{INS\text{-}GFP}$ using TALENS as previously described[45] (Supplementary Figure 6, henceforth referred to as Mel1$^{INS\text{-}GFP;AAVS1\text{-}Luc}$). Six weeks following transplantation, we observed pervasive teratomas in the animals that were transplanted with naked hES under the kidney capsule and an increase in body weight indicative of increased tumor mass in these animals (Figures 4C,D). In addition, imaging of luciferase signal demonstrates the confinement of encapsulated cells, whereas naked Mel1$^{INS\text{-}GFP;AAVS1\text{-}Luc}$ escaped the kidney capsule and were detected throughout the peritoneal body cavity (Figure 4D,F). Furthermore, H&E staining and immunostainings of tissue section grafts show that human teratoma cells are well confined within the device margins (Supplementary Figure 7A,B). Taken together, these data demonstrate the ability of our PCL NID encapsulation approach to contain proliferative cell populations within the device and prevent them from spreading throughout the body.

In Vivo Viability and Function of hES-βC Encapsulated in NID

To study viability and function of encapsulated Mel1$^{INS\text{-}GFP;AAVS1\text{-}Luc}$ derived hES-βC into NID, we transplanted them between the caudate lobe and left hepatic lobe of NSG mice, as this site was determined to be the most optimal transplant site for cell survival (Supplementary Figure 8A,B). The liver is one of the main sites of action of insulin and has been explored as an attractive site for islet transplantations due to its large surface area and ample vascularization.[46] We measured graft persistence using bioluminescence imaging of the constitutively expressed luciferase gene. Luciferase bioluminescence in mice transplanted with NID-encapsulated hES-βC was detected on day of transplantation as well as 30 days and 6 months after transplantation (Figure 5A,E). These results are in agreement with our *in vitro* data showing that NIDs allow the long-term survival of hES-βC cells. To assess the functional properties of encapsulated hES-βC 1 week post-transplantation, mice were fasted overnight, followed by a challenge consisting of a bolus of glucose *via*

intraperitoneal injection. Glucose-stimulated C-peptide production can be seen 1 week after transplantation into NSG mice and remained constant at 6 months (Figure 5B). The long-term function of NID-encapsulated grafts was similarly assessed. Mouse serum was collected following overnight fast and 1 h after intraperitoneal glucose challenge and measured for human C-peptide concentration. Glucose-stimulated C-peptide secretion can be demonstrated in all mice, and glucose stimulation index ranged from 2 to 7 (Figure 5C,D). Quantification of bioluminescence intensity at day 0 and 6 months following transplantation of NID-encapsulated cells shows approximately 75% graft loss (Figure 5F). This degree of graft loss is expected and comparable with graft loss observed when unencapsulated hES-βCs are transplanted in the subcutaneous space (data not shown). Explantation of NID devices containing hES-βC cells after 6 months followed by immunostaining for human C-peptide shows islet-like clusters within the device (Figure 5G). Collectively, these studies show that NIDs are capable of supporting the viability and function of hES-βC *in vivo* for at least 6 months.

In Vivo Evaluation of Immunoisolation by NID Encapsulation

Because T cells are the principal drivers of alloimmune rejection of grafts, immunoprotective cell encapsulation devices must be able to prevent their activation. To maximally assess the immunoisolation capability of NIDs *in vivo*, we measured activation of antigen-specific T cells in response to mice challenged with ovalbumin (OVA)-expressing B16 cells encapsulated in NIDs. OVA-specific CD8+ T cells were collected from lymph nodes of OT-1 T cell receptor transgenic mice,[47] stained with VPD-450, and adoptively transferred into wild-type C57BL/6J mice. The mice then received an intraperitoneal challenge of 2×10^7 free or NID-encapsulated OVA-expressing B16 melanoma cells. Six days following the challenge, draining lymph nodes and spleen were harvested and analyzed for the proliferation of OT1 OVA-specific T cells (Figure 6A). Flow cytometric analysis revealed loss of VPD-450 dye in mice with an unprotected B16-OVA challenge transplant, indicating extensive proliferation of OT1 cells; however, proliferation of OT1 T cells was minimal in mice that have been challenged with encapsulated B16-OVA cells (Figure 6B). Animals transplanted with encapsulated B16-OVA cells had significantly reduced OVA-specific T cell proliferation in both the spleen and draining lymph nodes (Figure 6C,D). Moreover, there was no significant difference between the median fluorescent intensity of OVA-specific T cell populations in animals that received NID-encapsulated B16-OVA cells when compared to animals that did not receive any B16-OVA cells (Figure 6E,F). These results definitively demonstrate the absence of allogeneic antigen-specific T cell priming in hosts that received encapsulated cell transplants.

CONCLUSIONS

Stem cell replacement therapy has the potential to fundamentally change the way we treat and manage diabetes by achieving insulin independence in patients. Significant progress has been made in developing human stem-cell-derived insulin-producing cells,[7–14] but ultimately stem cell products benefit from integration with device strategies in order to overcome translational challenges in cell delivery, engraftment, immunoprotection, and safety.[17] Although there have been several encouraging reports of encapsulation strategies

achieving glucose correction in animal models, we still have much to learn about the engineering specifications necessary for successful cell engraftment and immunoprotection.

In this report, we systematically evaluate a bilaminar synthetic polymer nanoporous immunoprotective cell encapsulation device (NID) for its ability to immunoprotect and sustain the function and viability of human stem-cell-derived β-cells both *in vitro* and *in vivo*. The use of stem-cell-derived β-cell products in this study mitigates existing islet donor shortages and potentially enables more diabetic patients to receive cell replacement therapy. Macroencapsulation devices offer distinct translational advantages of teratoma confinement and retrievability compared to microencapsulation alternatives. Microencapsulation approaches using sodium alginate typically experience thick fibrous capsule formation, whereas macroencapsulation NIDs in our study show robust neovascularization with minimal foreign body response after long-term implantation. Immunoisolation studies demonstrate NIDs can robustly prevent antigen-specific T cell priming. Most importantly, 6 month animal studies demonstrate that hSC-βC in NID are both glucose-responsive and viable with a GSI index that exceeds the minimum standard for islet transplantation currently performed clinically. A better understanding of the parameters necessary for efficient engraftment and immunoprotection of cells in encapsulation devices will greatly improve the chances of successfully bringing β-cell replacement therapies into the clinic.

METHODS

Nanoporous Immunoprotective Device Fabrication

Chemicals were purchased from Sigma-Aldrich unless noted. All films were spun-cast onto silicon wafers at 1000 rpm for 30 s, followed by 2000 rpm for 30 s. Nanoporous polycaprolactone (80 kDa Mn) films were fabricated using an established template-based approach reported elsewhere.[25] In brief, a 0.5 M solution of zinc acetate dihydrate and ethanolamine in 2-methoxyethanol was spun-cast onto silicon wafers and annealed at 300 °C on a hot plate to generate a zinc oxide (ZnO) seed layer. From this seed layer, ZnO nanorods were hydrothermally grown in a 5 mM zinc acetate solution at 85 to 90 °C for 2 h. A 150 mg/mL PCL solution was then spun-cast onto the nanorods, followed by a 150 mg/mL PEG:PCL solution to provide a microporous support, creating a nanoporous film with a microporous backing support layer. The film was soaked in a dilute sulfuric acid solution to etch away the ZnO nanorods and also dissolve the PEG, resulting in a nanoporous membrane with pores ranging from 30 to 100 nm supported by a microporous backing. Membrane characterizations and ZnO nanorod morphology were previously measured.[25] To assemble the device, two PCL thin films were heat-sealed together using resistive heating of a nichrome wire. A two-step heat-sealing method was used where a 1.2 A current ran through a nichrome wire outlining the regions to be sealed. For the first sealing step, two films were placed over a U-shaped nichrome wire embedded in PDMS (Sylgard 184), 1 cm in diameter. To secure the membranes, a PDMS weight was placed over the films holding them flat. A 1.2 A current ran through the wire for 15 s and sealed the devices in the shape of a U, defining the device lumen shape and leaving an open side for cell injection. hSC-βC in high glucose Dulbecco's modified Eagle's medium (DMEM) were injected into the

devices through the remaining open side and sealed by placing the open edge over a straight nichrome wire embedded in PDMS and heat-sealed with a 1.2 A current for 10 s.

Scanning Electron Microscopy

Nanoporous PCL thin films were mounted on a flat SEM mount with colloidal graphite (Ted Pella). Cross sections were flash-dipped in isopropyl alcohol, followed by liquid nitrogen freeze fracture and then mounted. Samples were imaged by Carl Zeiss Ultra 55 field emission scanning electron microscope using an in-lens secondary electron detector at San Francisco State University.

Transwell Diffusion Assays

Standard Falcon brand 24-well 400 nm pore size PTFE transwell insert barriers were kept intact (PTFE-400) or removed and replaced with 20 nm pore size or 200 nm pore size immunoprotective films (NIM-20, NIM-200). The inserts were then placed into respective wells on a 24-well plate. For transport studies, 0.3 mL of 100 μg/mL FITC-conjugated dextran at 4, 10, and 40 kDa, 0.3 mL of 100 μg/mL human IgG, or 10 mM glucose solution in PBS was placed in the top compartment. One milliliter of PBS was placed in the bottom compartment. The transwell culture plate was placed in a 37 °C incubator and left for 7 days or 5 min (glucose transport). Solution from the top and bottom compartments was sampled, and concentration was quantified by a fluorimeter. Glucose detection kit (ab102617) was used to determine the glucose concentrations. For cytokine diffusion studies, media from 48 h cultured anti-CD3- and anti-CD28-activated splenocytes were collected and placed in the top compartment, and fresh medium was placed in the bottom compartment. After 7 day incubation at 37 °C, samples from both compartments were collected and quantified using mouse 31-plex cytokine Luminex kit.

Cell Culture

Isolation of mouse islets was performed as described.[48] Islets were cultured in RPMI 1640 supplemented with 10% (v/v) fetal bovine serum. Splenocytes were isolated from C57BL/6J mice by passing crushed spleen through a filter mesh and cultured in DMEM supplemented with 5% (v/v) fetal bovine serum.

Undifferentiated Mel1$^{\text{INS-GFP}}$ cells[37] were maintained on mouse embryo fibroblast feeder layers (Millipore) in hESC media as described.[13] Suspension-based direct differentiations to generate hES-βC were carried out as described[8] with improvements to the last stage based on published reports.[36,49]

Gene Targeting of Mel1$^{\text{INS-GFP}}$ Cells

To generate a cell line that expresses a constitutive firefly luciferase gene, we employed a recently published gene-targeting approach of the insulated human AAVS1 loci employing TALENs.[45] Briefly, we amplified a 6332 bp DNA piece containing all bacterial components, both homologies to the human AAVS1 loci, as well as the puromycin resistance gene from the Puro-Cas9 donor plasmid (Addgene #58409) and cloned a fragment consisting of a peptide cleavage site T2A, followed by the firefly luciferase gene and a poly-A sequence in, to recirculate the DNA piece. The resulting plasmid, termed Puro-T2A-Luc donor, was

sequence verified by sanger sequencing. Confluent Mel1$^{INS-GFP}$ were dissociated to single cells, and approximately 8.0 × 10^6 cells were mixed with 5 μg of each of the TALEN plasmids and 20 μg of the Puro-T2A-Luc donor in a 0.4 cm gap electro-cuvette (Biorad). Cells were electroporated using a GenePulser (Biorad) using an exponential decay with 250 V and 500 μF settings. Targeted cells were plated on DR4-resistant MEFs, and clones were selected with 0.5 μg/mL puromycin for 4 days. After 11–12 days, individual clones were manually picked and expanded before freeze down and genomic DNA analysis. gDNA was analyzed with primers for WT and correct Puro integration. WT/Puro forward: CCG GAA CTC TGC CCT CTA AC, WT reverse: AGA TGG CTC CAG GAA ATG GG, Puro reverse: GTG GGC TTG TAC TCG GTC AT. Mel1$^{INS-GFP,AAVS1-Luc}$ line #3 was used for direct differentiation experiments.

Mice

NOD.Cg-Prkdcscid Il2rgtm1Wjl/SzJ mice (NSG) and C57BL/6J mice were obtained from Jackson Laboratories. Mice use in this study were maintained according to protocols approved by the University of California, San Francisco, Committee on Laboratory Animal Resource Center. For kidney capsule grafts, approximately 2.0 × 10^6 hESC-differentiated cells in clusters were transplanted as described.[44] For encapsulated grafts, approximately 2.0 × 10^6 hESC-differentiated cell clusters encapsulated in a bilaminar nanoporous immunoprotective device were transplanted between the caudate and left hepatic lobe. For glucose-induced insulin secretion, mice were fasted overnight and serum was collected before and 1 h after intraperitoneal administration of 3 g/kg D-glucose solution. Serum C-peptide levels were quantified by ELISA using a commercially available kit (Alpco).

Flow Cytometric Analysis

Briefly, spheres were collected and allowed to settle by gravity. Clusters were washed once in PBS and dissociated by gentle pipetting after 12–15 min incubation in Accumax (Innovative Cell Technologies). For flow-based analysis, dissociated cells were fixed with 4% paraformaldehyde (Electron Microscopy Science) for 15 min at room temperature, followed by two washes in PBS. Samples were either stored at 4 °C or immediately stained with directly conjugated antibodies. Data analysis was performed with FlowJo software. NKX6.1-Alexa 647, PDX1-PE were obtained from BD Bioscience, and a human C-peptide antibody (Millipore, CHU-09) was in-house conjugated to Alexa 488 fluorophore using a commercially available kit (Invitrogen).

Glucose-Stimulated Insulin Secretion

Free and encapsulated hESC-derived spheres were transferred into tubes and washed twice with Krebs–Ringer bicarbonate buffer (KRB) containing 2 mM glucose. Samples were incubated for 1 h in 2 mM glucose containing KRB to allow equilibration of cells. Two millimoles of buffer was removed and replaced with fresh KRB containing 2 mM glucose for 30 min followed by incubation for another 30 min in KRB containing 20 mM glucose. After the incubation period, buffers were collected for human C-peptide-specific ELISA analysis using a commercially available kit (Alpco).

Immunostaining

Mouse tissue samples were collected and fixed in 4% paraformaldehyde for 24 h and washed with phosphate buffered saline at 4 °C for 48 h then 30% sucrose for 24 h. Tissue samples were embedded in optimal cutting temperature and sectioned for staining. COL1A1, F4/80, and vWF antibodies were purchased from BD Biosciences. Antimitochondria antibodies were purchased from Millipore.

In Vivo Bioluminescence Imaging

Nanoporous immunoprotective devices encapsulated with luciferase-expressing human embryonic cell-derived pancreatic β-like cell clusters (hSC-βC) were implanted between the caudate and left hepatic lobes of the liver of NOD.Cg-Prkdcscid Ill2rgtm1Wjl/SxJ (NSG) mice. Survival of the encapsulated cells in vivo was assessed by monitoring luciferase activity using a Xenogene IVIS 200 imaging system (PerkinElmer). The animals transplanted with hSC-βC cells were injected IP with D-luciferin solution (Goldbio, St. Louis, MO) at the dose of 150 mg/kg 5 min before imaging to capture the peak in bioluminescent intensity. The mice were anesthetized with an isoflurane mixture (2% in 98% O_2) and imaged using a Xenogen IVIS 200 imaging system. Bioluminescence images were acquired for 3 min and then analyzed using the Living Image analysis software (Xenogen, Alameda, CA). Regions of interest (ROI) were centered over the bioluminescence regions. Photons were counted within the ROI over the acquisition time. Adherence to the same imaging protocol ensured consistent signal detection on different days of *in vivo* imaging.

Cell Transfer

One day before cell transplantation, mice received violet proliferation dye (VPD-450)-labeled lymph node (LN) cells from Ub-GFP-OT-1 Tg mice *via* retro-orbital injection as previously described.[50] Six days after the transplant, pancreatic draining lymph node and the spleen were harvested, and the proliferation of transferred T cells was determined using flow cytometry by measuring the dilution of CFSE. A Fortessa flow cytometer (BD Biosciences, San Jose, CA) and FACSDiva software (BD Biosciences) were used for flow cytometric analysis. For sensitization of B57CL/6J mice, OVA-expressing B16 melanoma cells were cultured overnight in DMEM with serum washed twice in PBS. Cells were irradiated at 10 gy, and 20×10^6 cells were injected IP or encapsulated into devices and transplanted into each recipient animal.

Supplementary Material

Refer to Web version on PubMed Central for supplementary material.

Acknowledgments

This work was supported, in part, by grants from JDRF. Microscopy analysis was performed at the Nikon Imaging Core at UCSF and Scanning Electron Microscopy facility at SFSU. Puro-Cas9 donor, AAVS1-TALEN-R, and -L were a gift from D. Huangfu (Addgene plasmid #59026, #59026, and #58409). B16-OVA cells and OT-1 TCR Tg mice were gifts from M.F. Krummel. We would like to thank J. Han for providing figure illustrations.

References

1. Melendez-ramirez LY, Cefalu WT, Richards RJ. Complications of Type 1 Diabetes. Endocrinol. Metab. Clin. North Am. 2010; 39:625–640. [PubMed: 20723824]
2. Shapiro AM, Lakey JR, Ryan EA, Korbutt GS, Toth E, Warnock GL, Kneteman NM, Rajotte RV. Islets Transplantation in Seven Patietns with Type 1 Diabetes Mellitus Using a Glucocorticoid-Free Immunosuppressive Regimen. N. Engl. J. Med. 2000; 343:230–238. [PubMed: 10911004]
3. Frassetto A, Masharani U, Kerlan RK, Fong L, Vincenti FG, Surgery T, Francisco S, Francisco S, States U. Islet Transplantation in Type 1 Diabetics Using an Immunosuppressive Protocol Based on the Anti-LFA-1 Antibody Efalizumab. Am. J. Transplant. 2010; 10:1870–1880. [PubMed: 20659093]
4. Barton FB. Improvement in Outcomes of Clinical Islet Transplantation: 1999 – 2010. Diabetes Care. 2012; 35:1436–1445. [PubMed: 22723582]
5. Ryan EA, Paty BW, Senior PA, Bigam D, Alfadhli E, Kneteman NM, Lakey JRT, Shapiro AMJ. Five-Year Follow-Up After Clinical Islet Transplantation. Diabetes. 2005; 54:2060. [PubMed: 15983207]
6. Bouwens L, Houbracken I, Mfopou JK. The Use of Stem Cells for Pancreatic Regeneration in Diabetes Mellitus. Nat. Rev. Endocrinol. 2013; 9:598–606. [PubMed: 23877422]
7. Zhou Q, Brown J, Kanarek A, Rajagopal J, Melton DA. In Vivo Reprogramming of Adult Pancreatic Exocrine Cells to B-Cells. Nature. 2008; 455:627. [PubMed: 18754011]
8. Russ HA, Parent AV, Ringler JJ, Hennings TG, Nair GG, Shveygert M, Guo T, Puri S, Haataja L, Cirulli V, Blelloch R, Szot GL, Arvan P, Hebrok M. Controlled Induction of Human Pancreatic Progenitors Produces Functional Beta-like Cells. EMBO J. 2015; 34:1759–1772. [PubMed: 25908839]
9. Hebrok M. Generating β Cells from Stem Cells-the Story so Far. Cold Spring Harbor Perspect. Med. 2012; 2:a007674.
10. Nostro MC, Keller G. Seminars in Cell & Developmental Biology Generation of Beta Cells from Human Pluripotent Stem Cells: Potential for Regenerative Medicine. Semin. Cell Dev. Biol. 2012; 23:701–710. [PubMed: 22750147]
11. D'Amour, Ka, Agulnick, AD., Eliazer, S., Kelly, OG., Kroon, E., Baetge, EE. Efficient Differentiation of Human Embryonic Stem Cells to Definitive Endoderm. Nat. Biotechnol. 2005; 23:1534–1541. [PubMed: 16258519]
12. Van Hoof D, Mendelsohn AD, Seerke R, Desai Ta, German MS. Differentiation of Human Embryonic Stem Cells into Pancreatic Endoderm in Patterned Size-Controlled Clusters. Stem Cell Res. 2011; 6:276–285. [PubMed: 21513906]
13. Guo T, Landsman L, Li N, Hebrok M. Factors Expressed by Murine Embryonic Pancreatic Mesenchyme Enhance Generation of Insulin-Producing Cells from hESCs. Diabetes. 2013; 62:1581–1592. [PubMed: 23305648]
14. Rezania A, Bruin JE, Arora P, Rubin A, Batushansky I, Asadi A, O'Dwyer S, Quiskamp N, Mojibian M, Albrecht T, Yang YHC, Johnson JD, Kieffer TJ. Reversal of Diabetes with Insulin-Producing Cells Derived in Vitro from Human Pluripotent Stem Cells. Nat. Biotechnol. 2014; 32:1121–1134. [PubMed: 25211370]
15. Steele, JaM, Hallé, J-P., Poncelet, D., Neufeld, RJ. Therapeutic Cell Encapsulation Techniques and Applications in Diabetes. Adv. Drug Delivery Rev. 2014; 67–68:74–83.
16. Soon-Shiong P, Feldman E, Nelson R, Heintz R, Yao Q, Yao Z, Zheng T, Merideth N, Skjak-braek G, Espevik T. Long-term reversal of diabetes by the injection of immunoprotected islets. Proc. Natl. Acad. Sci. U.S.A. 1993; 90:5843–5847. [PubMed: 8516335]
17. Desai T, Shea LD. Advances in Islet Encapsulation Technologies. Nat. Rev. Drug Discovery. 2016; 16:338–350. [PubMed: 28008169]
18. Pepper AR, Pawlick R, Gala-lopez B, Macgillivary A, Mazzuca DM, White DJG, Toleikis PM, Shapiro AMJ. Diabetes Is Reversed in a Murine Model by Marginal Mass Syngeneic Islet Transplantation Using a Subcutaneous Cell Pouch Device. Transplantation. 2015; 99:2294. [PubMed: 26308506]

19. Lim F, Sun AM. Microencapsulated Islets as Bioartificial Endocrine Pancreas. American Association for the Advancement of Science. 2016; 210:908–910. http://www.jstor.org/stable/1684447.
20. Duvivier-Kali VF, Omer a, Parent RJ, O'Neil JJ, Weir GC. Complete Protection of Islets against Allorejection and Autoimmunity by a Simple Barium-Alginate Membrane. Diabetes. 2001; 50:1698–1705. [PubMed: 11473027]
21. Vegas AJ, Veiseh O, Gürtler M, Millman JR, Pagliuca FW, Bader AR, Doloff JC, Li J, Chen M, Olejnik K, Tam HH, Jhunjhunwala S, Langan E, Aresta-dasilva S, Gandham S, Mcgarrigle JJ, Bochenek MA, Hollister-lock J, Oberholzer J, Greiner DL. Long-Term Glycemic Control Using Polymer- Encapsulated Human Stem Cell-Derived Beta Cells in Immune-Competent Mice. Nat. Med. 2016; 22:306. [PubMed: 26808346]
22. Scharp DW, Marchetti P. Encapsulated Islets for Diabetes Therapy: History, Current Progress, and Critical Issues Requiring Solution. Adv. Drug Delivery Rev. 2014; 67–68:35–73.
23. Colton CK. Oxygen Supply to Encapsulated Therapeutic Cells. Adv. Drug Delivery Rev. 2014; 67–68:93–110.
24. Weir GC. Islet Encapsulation: Advances and Obstacles. Diabetologia. 2013; 56:1458–1461. [PubMed: 23636639]
25. Bernards, Da, Desai, Ta. Nanotemplating of Biodegradable Polymer Membranes for Constant-Rate Drug Delivery. Adv. Mater. 2010; 22:2358–2362. [PubMed: 20376851]
26. Nyitray CE, Chang R, Faleo G, Lance KD, Bernards DA, Tang Q, Desai TA. Polycaprolactone Thin-Film. ACS Nano. 2015; 9:5675–5682. [PubMed: 25950860]
27. Chroboczek Kelker H, Le J, Rubin BY, Yip YK, Nagler C. Three Molecular Weight Forms of Natural Human Interferon-γ Revealed by Immunoprecipitation with Monoclonal Antibody. J. Biol. Chem. 1984; 259:4301–4304. [PubMed: 6423641]
28. Beutler B, Greenwald D, Hulmes JD, Chang M, Pan Y-CE, Mathison J, Ulevitch R, Cerami A. Identity of Tumour Necrosis Factor and the Macrophage-Secreted Factor Cachectin. Nature. 1985; 316:552–554. [PubMed: 2993897]
29. Hailey, KL. Ph.D. Thesis. UC San Diego: 2010. The Expanding Folding/functional Landscape of the Interleukin-1 Family.
30. Woodruff MA, Hutmacher DW. The Return of a Forgotten polymer—Polycaprolactone in the 21st Century. Prog. Polym. Sci. 2010; 35:1217–1256.
31. Yuan S, Xiong G, Wang X, Zhang S, Choong C. Surface Modification of Polycaprolactone Substrates Using Collagen-Conjugated Poly(methacrylic Acid) Brushes for the Regulation of Cell Proliferation and Endothelialisation. J. Mater. Chem. 2012; 22:13039.
32. Labet M, Thielemans W. Chem. Soc. Rev. 2009; 38:3484–3504. [PubMed: 20449064]
33. Hamilton RG. The Human IgG Subclasses. 2001
34. Itkin-ansari, P., Levine, F. Annals of the New York Academy of Sciences. Nov. 2003 Cell-Based Therapies for Diabetes: Progress towards a Transplantable Human Cell Line Article.
35. Djoba Siawaya JF, Siawaya D, Roberts T, Babb C, Black G, Golakai HJ, Bapela NB, Hoal E, Parida S, van Helden P, et al. An Evaluation of Commercial Fluorescent Bead-Based Luminex Cytokine Assays. PLoS One. 2008; 3:e2535. [PubMed: 18596971]
36. Pagliuca FW, Millman JR, Gürtler M, Segel M, Van Dervort A, Ryu JH, Peterson QP, Greiner D, Melton DA. Generation of Functional Human Pancreatic β Cells. Cell. 2014; 159:428–439. [PubMed: 25303535]
37. Micallef SJ, Li X, Schiesser JV, Hirst CE, Yu QC, Lim SM, et al. INS GFP/W Human Embryonic Stem Cells Facilitate Isolation of in Vitro Derived Insulin-Producing Cells. Diabetologia. 2012; 55:694–706. [PubMed: 22120512]
38. Taylor BL, Liu F-F, Sander M. Nkx6.1 Is Essential for Maintaining the Functional State of Pancreatic Beta Cells. Cell Rep. 2013; 4:1262–1275. [PubMed: 24035389]
39. Shih HP, Seymour PA, Patel NA, Yeo GW, Magnuson MA, Sander M, Xie R, Wang A, Liu PP, et al. A Gene Regulatory Network Cooperatively Controlled by Pdx1 and Sox9 Governs Lineage Allocation of Foregut Progenitor Cells. Cell Rep. 2015; 13:326–336. [PubMed: 26440894]
40. Krishnan R, Alexander M, Robles L, Foster CE, Lakey JRT. Islet and Stem Cell Encapsulation for Clinical Transplantation. Rev. Diabet. Stud. 2014; 11:84–101. [PubMed: 25148368]

41. Anderson JM, Rodriguez A, Chang DT. Foreign Body Reaction to Biomaterials. Semin. Immunol. 2008; 20:86–100. [PubMed: 18162407]
42. Brown BN, Ratner BD, Goodman SB, Amar S, Badylak SF. Macrophage Polarization: An Opportunity for Improved Outcomes in Biomaterials and Regenerative Medicine. Biomaterials. 2012; 33:3792–3802. [PubMed: 22386919]
43. Hentze H, Soong P, Wang S, Phillips BW, Putti TC, Dunn NR. Teratoma Formation by Human Embryonic Stem Cells: Evaluation of Essential Parameters for Future Safety Studies. Stem Cell Res. 2009; 2:198–210. [PubMed: 19393593]
44. Szot GL, Koudria P, Bluestone JA. Transplantation of Pancreatic Islets Into the Kidney Capsule of Diabetic Mice. J. Visualized Exp. 2007; 404
45. Zhu Z, González F, Huangfu D. The iCRISPR Platform for Rapid Genome Editing in Human Pluripotent Stem Cells. Methods Enzymol. 2014; 546:215. [PubMed: 25398343]
46. Cantarelli E, Piemonti L. Alternative Transplantation Sites for Pancreatic Islet Grafts. Curr. Diabetes Rep. 2011; 11:364–374.
47. Clarke R. Characterization of the Ovalbumin-Specific TCR Transgenic Line OT-I: MHC Elements for Positive and Negative Selection. Immunol. Cell Biol. 2000; 78:110–117. [PubMed: 10762410]
48. Li D, Yuan Y, Tu H, Liang Q, Dai L. A Protocol for Islet Isolation from Mouse Pancreas. Nat. Protoc. 2009; 4:1649–1652. [PubMed: 19876025]
49. Bruin JE, Rezania A, Xu J, Narayan K, Fox JK, O'Neil JJ, Kieffer TJ. Maturation and Function of Human Embryonic Stem Cell-Derived Pancreatic Progenitors in Macroencapsulation Devices Following Transplant into Mice. Diabetologia. 2013; 56:1987–1998. [PubMed: 23771205]
50. Thompson ED, Enriquez HL, Fu Y, Engelhard VH. Tumor Masses Support Naive T Cell Infiltration. J. Exp. Med. 2010; 207:1791–1804. [PubMed: 20660615]

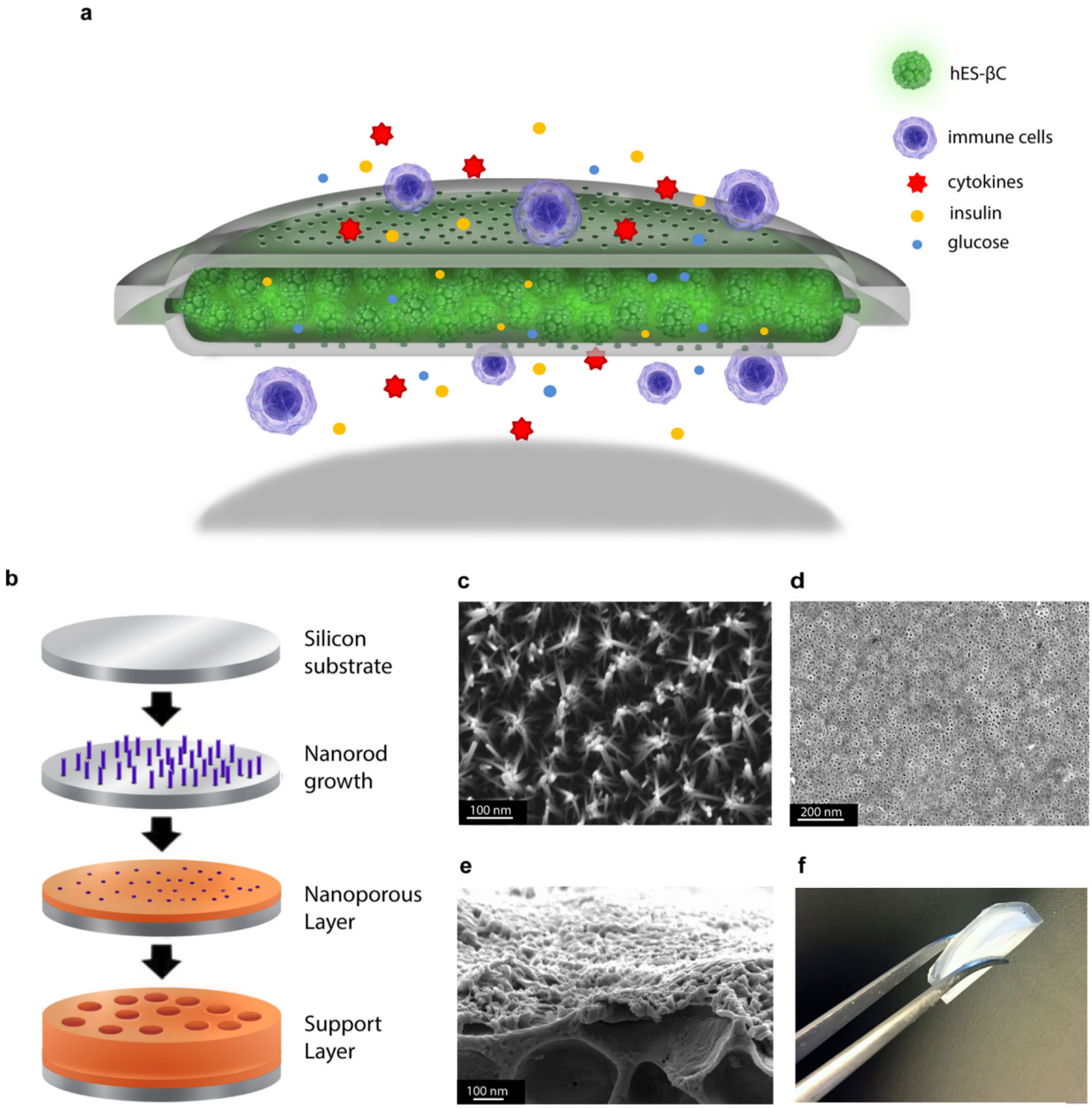

Figure 1.

Immunoprotective cell encapsulation device design and fabrication. (a) Illustration of immune-protective cell encapsulation device. (b) Schematic illustration of fabrication process for nanoporous thin films by zinc oxide nanorod growths and polymer templating. (c) Scanning electron microscopy image of zinc oxide nanorod templated silicon substrate. (d) Scanning electron microscopy image of the cross section of nanoporous caprolactone membrane. (e) Scanning electron microscopy image of nanopores on the surface of the polycaprolactone membrane. (f) Assembled immunoprotective cell encapsulation device.

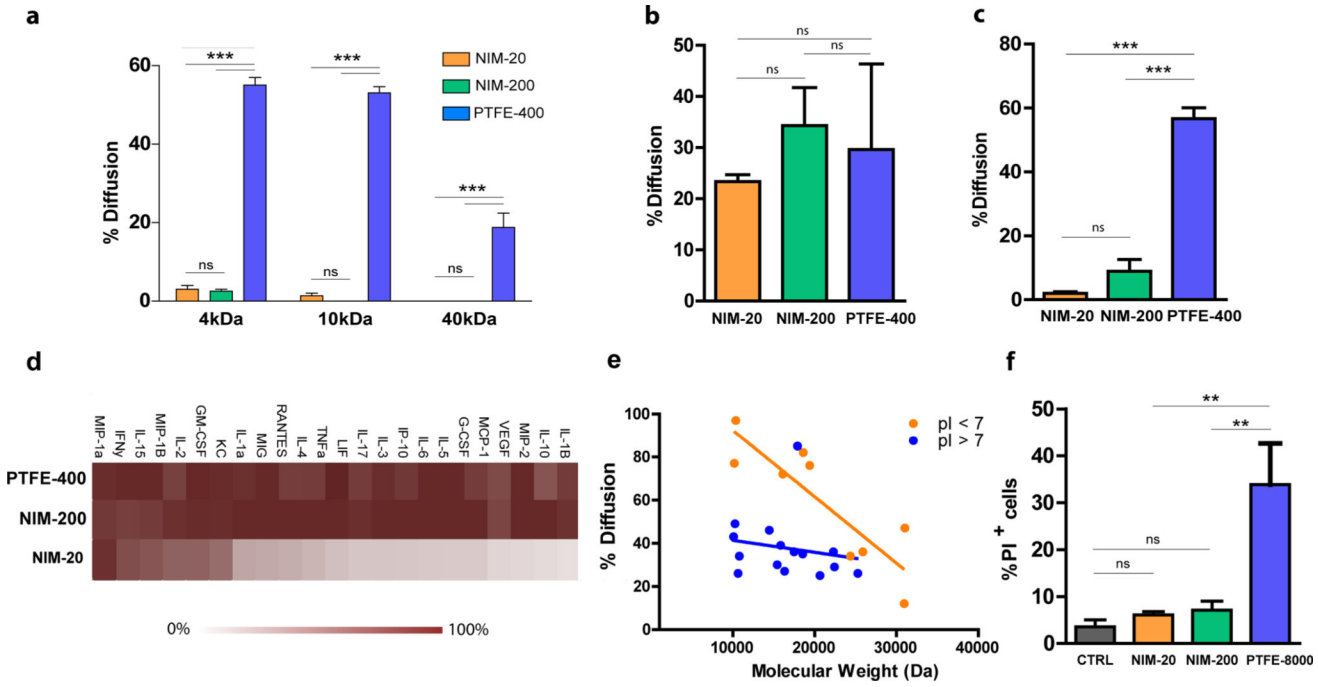

Figure 2.

In vitro characterization of nanoporous immunoprotective membranes. (a) 4, 10, and 40 kDa FITC-dextran diffusion rate across NIM-20, NIM-200, and PTFE-400 pore size films over 7 days ($n = 5$ per group). (b) 5 min glucose diffusion rate across NIM-20, NIM-200, and PTFE-400 ($n = 5$ per group). (c) FITC-IgG diffusion rate across NIM-20, NIM-200, and PTFE-400 films over 7 days ($n = 6$ per group). (d) Quantification of transwell proinflammatory cytokine diffusion across NIM-20, NIM-200, and PTFE-400 over 7 days measured by Luminex. (e) Cytokine diffusion rate for NIM-20 compared to molecular weight and protein charge. (f) Propidium iodine staining of dissociated islets recovered from coculture with anti-CD3/CD28-activated splenocytes isolated from wild-type C57BL6/J mice separated by NIM-20, NIM-200, and PTFE-8000 or no splenocyte control (ctrl) over a 48 h period ($n = 3$ per group). $*P < 0.05$, $**P < 0.01$, $***P < 0.001$.

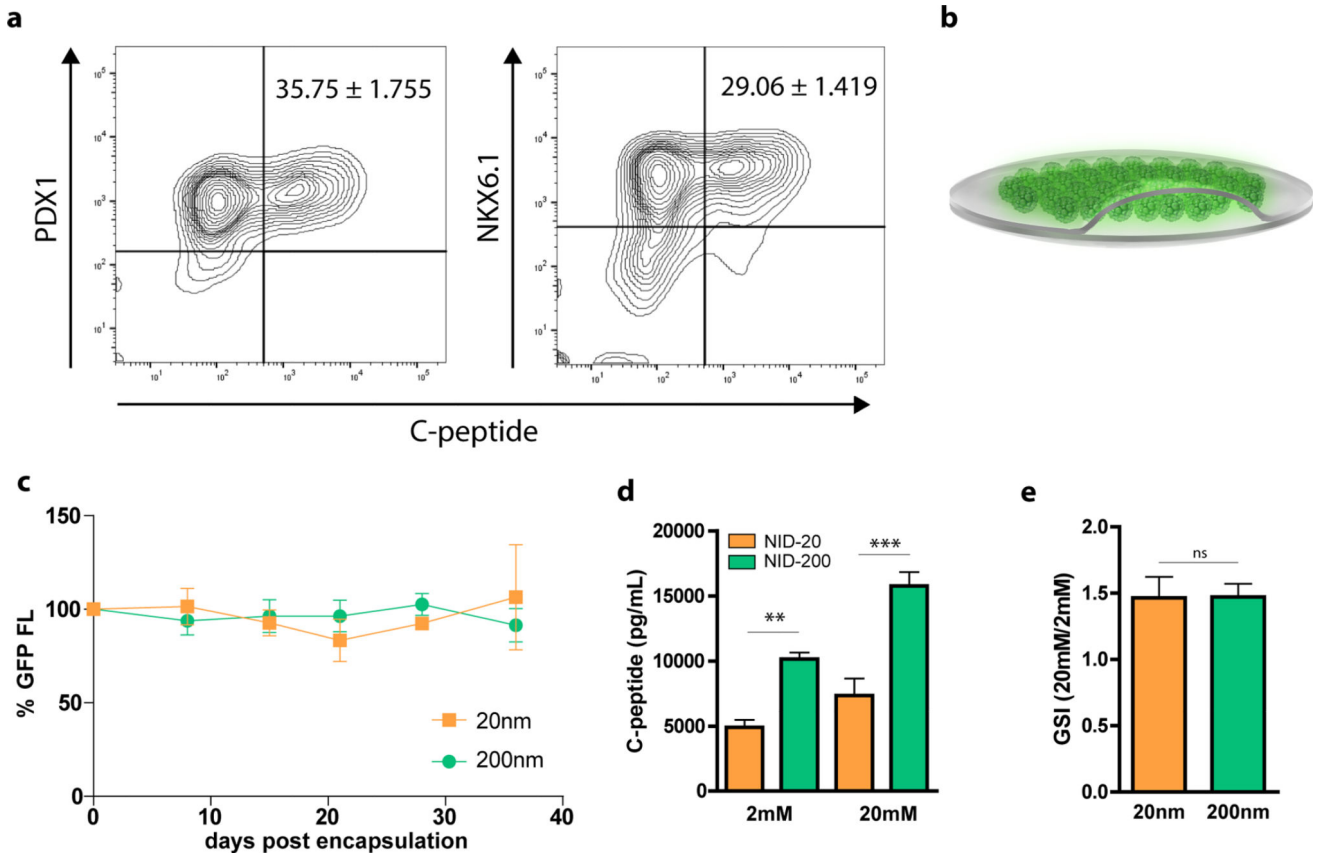

Figure 3.

In vitro evaluation of cell viability and function in nanoporous immunoprotective device. (a) Cytoflow-based co-analysis of intracellular β-cell transcription factors PDX1, NKX6.1, and the endogenous insulin synthesis marker C-peptide ($n = 8$). (b) Illustration of encapsulated hES$^{INS\text{-}GFP}$ derived β-cell-containing clusters in bilaminar thin film device. (c) GFP fluorescence signals measured from hES$^{INS\text{-}GFP}$-βC that were encapsulated in NID-20 and NID-200 and cultured for >5 weeks *in vitro* ($n = 4$) per group. (d) Glucose-stimulated insulin secretion assay for NID-20- and NID-200-encapsulated hES$^{INS\text{-}GFP}$-βC analyzed by human C-peptide specific ELISA ($n = 4$ per group). (e) Glucose stimulation index (GSI, 20 mM/2 mM glucose for 30 min) of NID-20- and NID-200-encapsulated hES$^{INS\text{-}GFP}$-βC ($n = 4$ per group). *$P < 0.05$, **$P < 0.01$, ***$P < 0.001$.

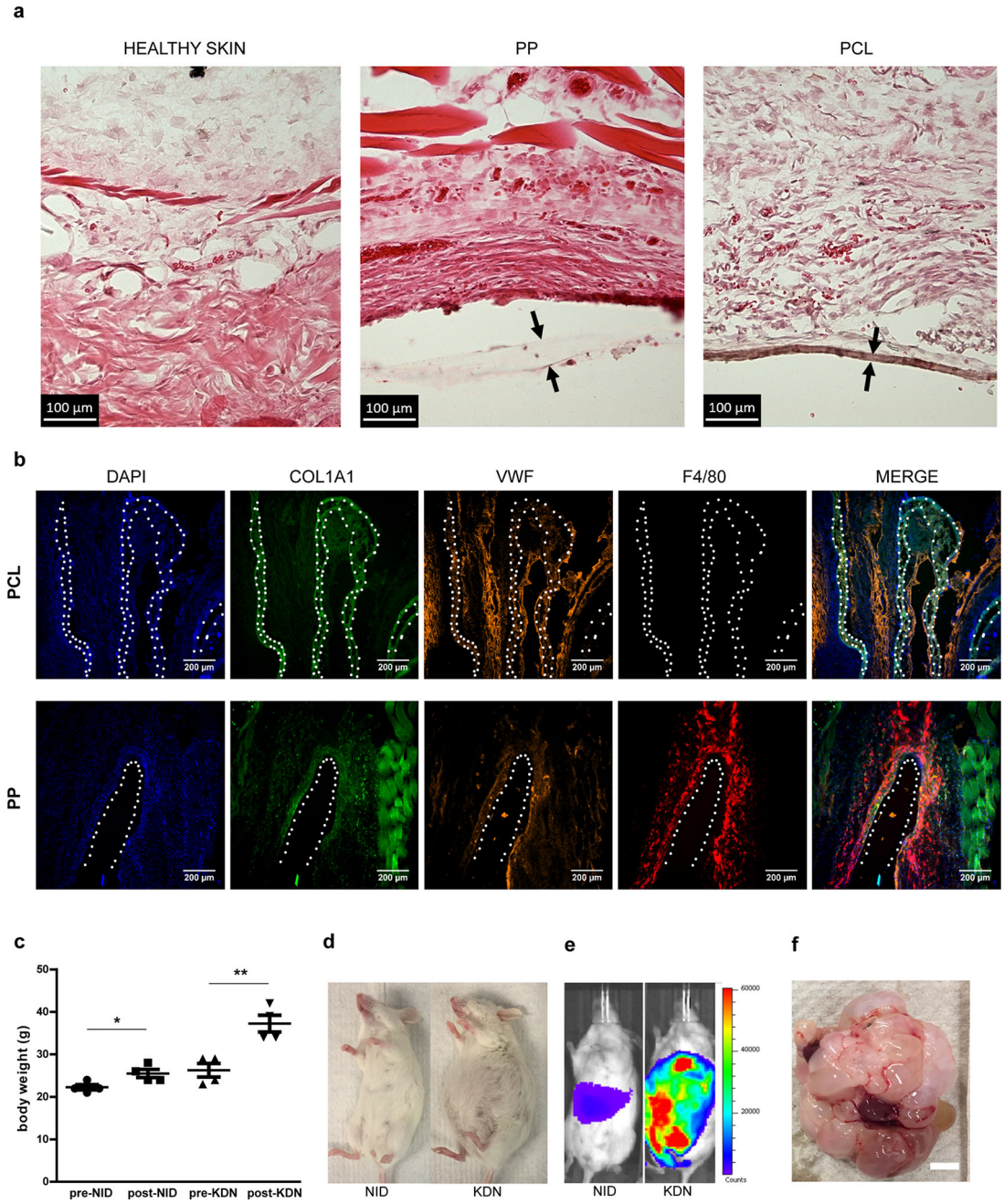

Figure 4.

In vivo NID biocompatibility and prevention of teratoma escape. (a) H&E stains of tissue sections of healthy skin, polypropylene, and polycaprolactone, with the solid arrows pointed toward the polymer membrane. (b) Immunofluorescent staining for collagen (COL1A1), neovasculature (vWF), and macrophage (F4/80) markers of 4 month subcutaneous polycaprolactone and polypropylene thin film implants in C57BL/6J mice. The white dotted lines delineate the location of the polymer membrane implant. (c) Day 0 and week 6 body weight measurements from mice transplanted with undifferentiated Mel1$^{INS\text{-}GFP;AAVS1\text{-}LUC}$ cells in NID or naked under the kidney capsule of NSG mice ($n = 4$ per group). *$P < 0.05$,

** $P < 0.01$, *** $P < 0.001$. (d) Gross image of mice that received undifferentiated $Mel1^{INS\text{-}GFP;AAVS1\text{-}LUC}$ cell transplants either encapsulated devices (NID) or naked (KDN) under the kidney capsule of NSG mice. (e) Representative bioluminescence image of NSG mice transplanted with undifferentiated $Mel1^{INS\text{-}GFP;CON\text{-}LUC}$ cells either encapsulated (NID) or naked (KDN) under the kidney capsule of NSG mice after 6 weeks. (f) Representative gross morphology image of explanted teratoma mass from undifferentiated, naked $Mel1^{INS\text{-}GFP;AAVS1\text{-}LUC}$ cells (scale bar = 1 cm).

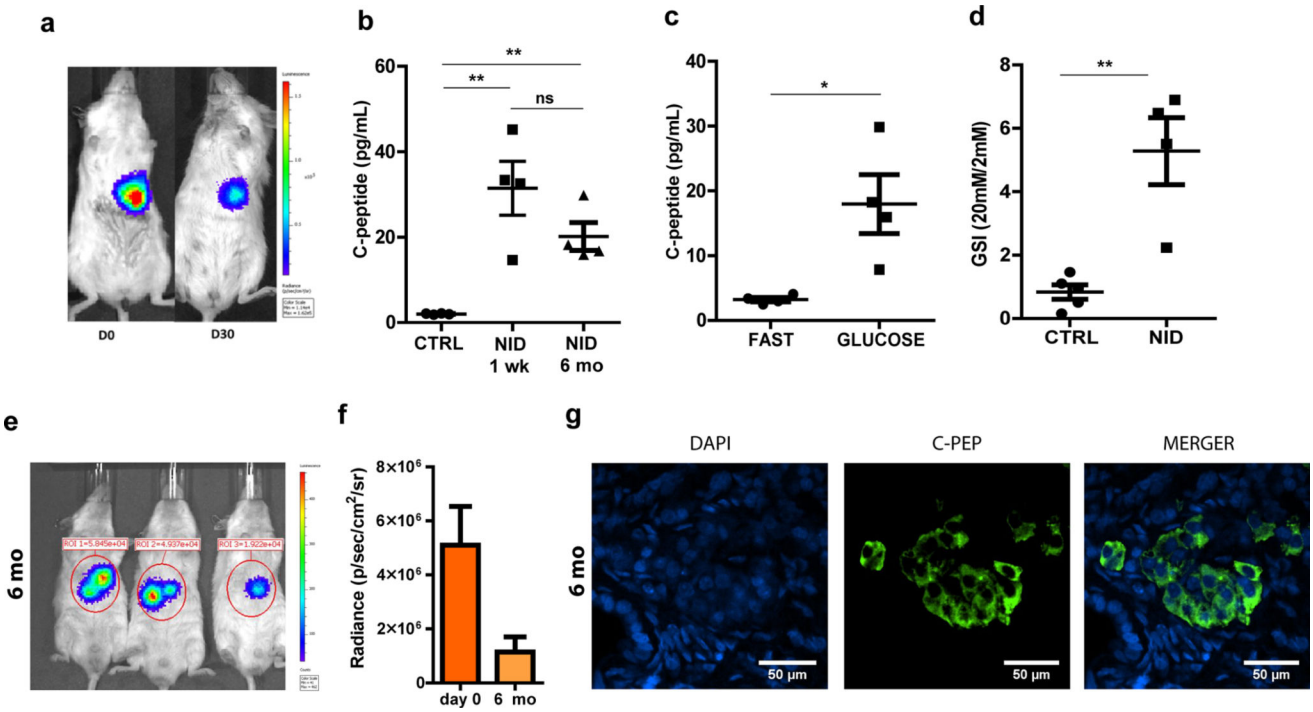

Figure 5.

In vivo viability of function of hES-βC encapsulated in NID. (a) Representative bioluminescence image of NSG mice transplanted with NID encapsulated hES$^{\text{INS-GFP;AAVS1-LUC}}$-$\beta$C between liver lobes at day 0 and day 30. (b) Human C-peptide concentration in mouse sera after 60 min IP glucose challenge of overnight fasted mice 1 week and 6 months post-transplantation of NID-encapsulated (NID) or untransplanted mice (CTRL) ($n = 4$ per group). (c) Guman C-peptide concentration in mouse sera after 60 min IP glucose challenge of overnight fasted mice 6 months post-transplantation of NID-encapsulated hES$^{\text{INS-GFP;AAVS1-LUC}}$-$\beta$Cs ($n = 4$ per group). (d) Glucose stimulation index (GSI) of NID-encapsulated or naked hES$^{\text{INS-GFP;AAVS1-LUC}}$-$\beta$Cs (CTRL) 6 months post-transplantation ($n = 4$ per group). *$P < 0.05$, **$P < 0.01$, ***$P < 0.001$. (e) Representative bioluminescence image of NSG mice transplanted with NID encapsulated hES$^{\text{INS-GFP;AAVS1-LUC}}$-$\beta$Cs after 6 months. (f) Quantification of luciferase bioluminescent intensity measured from animals on day 0 and 6 months after encapsulated hES$^{\text{INS-GFP;AAVS1-LUC}}$-$\beta$Cs transplantation. (g) Representative immunofluorescence staining of NID-encapsulated hES$^{\text{INS-GFP;AAVS1-LUC}}$-$\beta$Cs for human C-peptide (C-PEP) 6 months post-transplantation. Nuclei are visualized by DAPI staining.

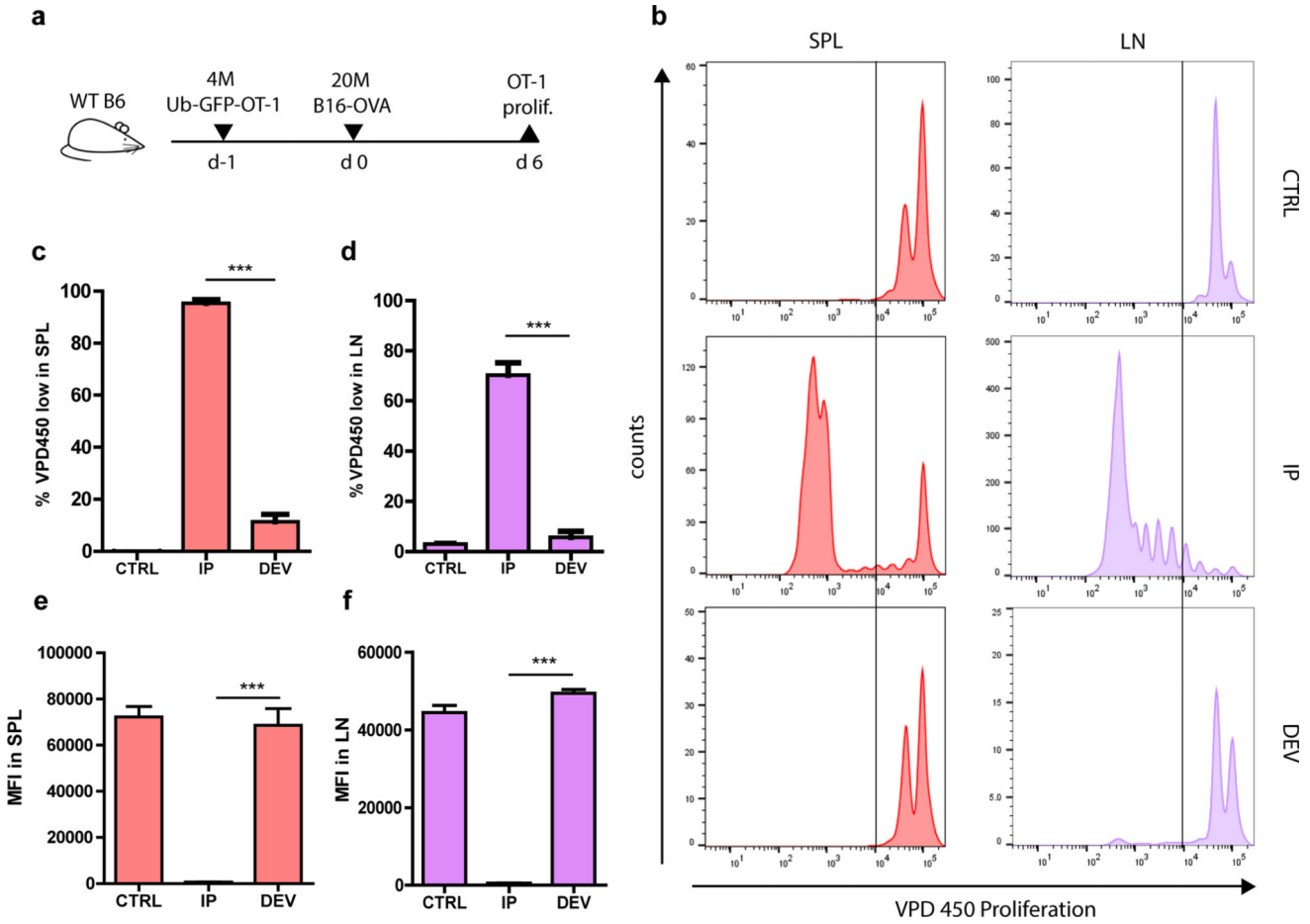

Figure 6.

In vivo evaluation of immune-isolation by NID encapsulation. (a–f) Wild-type C57BL/6J mice were adoptively transferred with 4×10^6 OT1-expressing $CD8^+$ T cells. The following day, mice received transplants of either NID-encapsulated or naked B16-OVA cells in the peritoneum. Spleen and draining lymph node were harvested 6 days later for analysis. (a) Schematic outlining the experimental approach. (b) Representative cell proliferation dye dilution graphs of $GFP^+/CD8^+$ T cells isolated from the spleen and lymph nodes of control mice (CTRL) or naked (IP) or NID-encapsulated (DEV) B16-OVA cells ($n = 3$ per group). (c) Quantification of proliferating antigen-specific T cells isolated from spleens of mice from CTRL, IP, and DEV conditions ($n = 3$ per group). (d) Quantification of proliferating antigen-specific T cells isolated from draining lymph nodes of mice from CTRL, IP, and DEV conditions ($n = 3$ per group). (e) Median fluorescence intensity measurement of $GFP^+/CD8^+$ T cells isolated from spleens of mice from CTRL, IP, and DEV conditions ($n = 3$). (f) Median fluorescence intensity measurement of $GFP^+/CD8^+$ T cells isolated from draining lymph nodes of mice from CTRL, IP, and DEV conditions ($n = 3$ per group). $^*P < 0.05$, $^{**}P < 0.01$, $^{***}P < 0.001$.